Journal of Agricultural Engineering

https://www.agroengineering.org/

Planar vector sequential extraction and harvesting optimization for dense quasi-spherical fruits: a low-damage and high-efficiency path balancing strategy based on improved NSGA-II

Shuzhen Yang,[1] Zhe Li,[1] Xiang Li,[1] Xiaohan Mei[2]

[1]School of Intelligent Manufacturing and Control Engineering;
[2]School of Mechatronic Engineering and Automation, Shanghai Polytechnic University, Shanghai, China

Corresponding author: Shuzhen Yang, School of Intelligent Manufacturing and Control Engineering, Shanghai Polytechnic University, Shanghai, China. E-mail: szyang@sspu.edu.cn

Please cite this article as doi: 10.4081/jae.2026.1935

Submitted: 3 May 2025
Accepted: 1 June 2026

Planar vector sequential extraction and harvesting optimization for dense quasi-spherical fruits: a low-damage and high-efficiency path balancing strategy based on improved NSGA-II

Shuzhen Yang,[1] Zhe Li,[1] Xiang Li,[1] Xiaohan Mei[2]

[1]School of Intelligent Manufacturing and Control Engineering;
[2]School of Mechatronic Engineering and Automation, Shanghai Polytechnic University, Shanghai, China

Corresponding author: Shuzhen Yang, School of Intelligent Manufacturing and Control Engineering, Shanghai Polytechnic University, Shanghai, China. E-mail: szyang@sspu.edu.cn

Availability of data and materials: the datasets used and/or analyzed during the current study are available from the corresponding author on reasonable request.

Competing interests: the authors declare that they have no competing interests.

Funding: this work was supported by the Shanghai Agricultural Science and Technology Innovation Project under Grant [I202303].

Authors' contributions: all authors contributed equally to: conceptualization, methodology, formal analysis, writing – original draft preparation, writing – review & editing, supervision. All authors read and approved the final version of the manuscript and agreed to be accountable for all aspects of the work.

Abstract

To address the challenges of excessive fruit damage and low success rates in densely clustered fruit harvesting requiring planar vector sequential extraction (a vector detachment strategy that projects 3D fruit positions onto the optimal operation plane for collision-free path planning, without restricting the end-effector to a fixed height plane), this study proposes a picking sequence optimization method based on multi-objective optimization. First, a geometric constraint model of critical tangent directions is established to determine collision-free detachment orientations for individual fruits. Subsequently, an Improved Non-dominated Sorting Genetic Algorithm II (I-NSGA-II) is developed by integrating multiple mechanisms: PSO-based extremum point injection for initial population generation, elitist selection for solution refinement, two-stage optimization (2-opt) for path smoothing, and cyclic crowding distance sorting for population diversity maintenance. This effectively resolves spatial

constraints in dense fruit cluster separation while improving damage-free harvesting success rates. Experimental results demonstrate that compared with standard NSGA-II, our method achieves a significant 2.5% reduction in collision failure rates across various fruit density clusters, with picking path lengths reduced to 55% of those obtained through single-objective optimization. The proposed approach effectively solves low-damage harvesting challenges in densely aggregated fruit regions, demonstrating substantial practical value for advancing robotic harvesting technologies.

Key words: Dense fruits; planar vector detachment method; damage-free harvesting; picking path optimization; improved NSGA-II.

Introduction

The mechanized harvesting of densely clustered fruits and vegetables (e.g., button mushrooms, kiwifruits, apples, citrus, and tomatoes) remains a critical challenge in modern agricultural production. These crops, characterized by fragile surface structures, dense spatial distributions, and complex three-dimensional morphologies, heavily rely on manual labor for traditional harvesting, leading to inefficiency, high costs, and seasonality constraints (Wang *et al*., 2022b). According to data from China's Ministry of Agriculture and Rural Development, the average monthly wage for rural migrant workers increased by over 150% from approximately 2,609 Chinese Yuan (about 333 Euros) in 2014 to 4,961 Chinese Yuan (about 633 Euros) in 2024, with seasonal labor costs being particularly prohibitive (source: National Bureau of Statistics of China, https://data.stats.gov.cn/dg/website/page.html#/pc/national/en/home). Fruit and vegetable harvesting robots, as pivotal components of smart agriculture, offer a promising solution (Chen *et al*., 2024). In recent years, breakthroughs in artificial intelligence, deep learning, soft robotics, and intelligent control have significantly advanced harvesting robots in end-effector dexterity, environmental adaptability, harvesting success rates, and efficiency, accelerating their transition from laboratory research to practical applications (Liu *et al*., 2022). Some prototypes have even approached commercial viability. For instance, Huang *et al*. (2024) developed a dual-arm apple harvesting robot with a field success rate of 76.97% and an average picking time of 7.29 s per fruit. MetoMotion's tomato harvesting robot reduced labor costs by 50% through multi-arm coordination (Matache *et al*., 2024). However, most harvesting robots remain far from practical adoption (Lehnert *et al*., 2018), especially for selective harvesting in dense fruit clusters (Xiong *et al*., 2019), where damage-free picking proves challenging and has become a major barrier to real-world deployment (Silwal *et al*., 2017).

When fruits adhere or overlap, they not only complicate visual segmentation and precise localization, thereby reducing harvesting success rates (Gong *et al*., 2022), but also create significant mechanical challenges. Mature target fruits surrounded by adjacent fruits hinder end-effector access, leading to harvesting failures. Additionally, detachment maneuvers may bruise adjacent fruits or displace their positions, further degrading harvesting performance. (Xiong *et al*., 2020) reported that while the success rate for harvesting isolated strawberries reached 96.8%, dense clusters limited this rate to 50-75% even with active obstacle avoidance algorithms. For fully occluded target fruits, the rate plummeted to 5%. Similar difficulties persist in mushroom, tomato, bell pepper, and kiwifruit harvesting.

Existing research on picking sequence optimization predominantly focuses on minimizing path lengths, exemplified by traditional ant colony algorithms (Kurtser *et al*., 2020). For instance, (Tang *et al*., 2020) proposed an improved immune algorithm (IIA) to optimize citrus harvesting paths, shortening both path length and time. Hu *et al*. (2019) utilized a modified particle swarm algorithm for shortest-path planning in button mushroom harvesting, while Wang *et al*. (2022a) optimized tea-picking sequences via a k-means-optimized genetic algorithm. While these methods improved efficiency, none addressed collision avoidance in dense clusters.

Wang *et al*. (2016) developed a bioinspired selective harvesting sequence planner based on visual saliency maps, prioritizing clusters by proximity and fruit count to reduce redundant motions. However, collision dynamics and intra-cluster sequence optimization were overlooked. Ning *et al*. (2022) applied density peaks clustering (DPC) with Gaussian kernel weighting to prioritize bell pepper clusters, preferentially harvesting outer-layer fruits to prevent collisions. Yet, this method struggled with complex nested fruit configurations. Dai *et al*. (2024) proposed a collision-free 3MSP2 sequence planning method for clustered tomatoes but omitted real-time ripeness detection, risking misjudgment of occluded fruits. Yang *et al*. (2022) combined genetic and ant colony algorithms to optimize multi-arm mushroom harvesting sequences, minimizing path lengths while adhering to height-based picking priorities. Although harvesting efficiency and success improved, the reliance on linear weighted multi-objective methods limited optimization efficacy. Notably, their fixed upward twisting detachment method avoided directional optimization, simplifying the problem.

The literature review reveals two critical gaps: limited research on picking sequence optimization incorporating damage-free detachment direction planning for dense fruits, and a lack of studies balancing both harvesting success rates (via collision-free separation) and efficiency (*via* path optimization). To address these gaps, this paper takes the quasi-planar densely clustered button mushrooms as the core research object, and proposes a novel multi-

objective optimization framework for dense fruit harvesting sequences with the following innovations: the proposed method optimizes detachment directions to prevent collisions during vector-based picking and plans sequences to maximize access to collision-free paths while minimizing travel distance, thereby enhancing both success rates and efficiency. The core geometric constraint model and multi-objective sequence optimization framework proposed in this study have the potential to be extended to 3D non-planar dense growth scenarios (e.g., kiwifruit and tomato) in subsequent research.

Optimal damage-free vector detachment direction determination principles of damage-free vector detachment

Fruit detachment methods, i.e., techniques to separate fruits from their nutrient sources, include pushing, pedicel cutting, twisting, and bending (Bu *et al*., 2020). Among these, pushing and bending (collectively termed vector detachment in this study) require sufficient directional clearance around the target fruit to avoid interference with adjacent fruits, thereby ensuring damage-free harvesting. The planar vector detachment method proposed in this study does not require the robotic end-effector to operate within a fixed height plane. For quasi-spherical fruits with height differences and inter-layer occlusion in 3D space (e.g., *Agaricus bisporus* fruiting bodies), we project the 3D spatial coordinates of fruits onto the optimal operation plane, and then carry out the vector detachment direction planning based on the 2D projection geometry. As illustrated in Figure 1a, many horticultural crops exhibit near-spherical geometries, which can be abstracted as circular cross-sections for detachment planning. In Figure 1b, red circles represent mature fruits requiring immediate harvesting, while blue circles denote immature fruits. For clarity, mushroom clusters are simplified in Figure 1c. Taking fruit f7 as an example, its dense surroundings—two mature and one immature neighbors—impose a high collision risk during arbitrary detachment attempts. However, selecting the optimal vector direction (indicated by arrows in Figure 1d) enables collision-free separation, minimizing damage and ensuring successful harvesting.

For densely clustered fruits, however, merely selecting an optimal vector direction is insufficient. Harvesting sequences must also be optimized to iteratively "unlock" spatial clearance for obstructed fruits. For instance, in Figure 1c, fruits f1, f4, f6, f8, f9, and f10 are initially blocked due to insufficient separation space. Adopting the sequence f7→f14→f16→f15→f12→f11→f10→f9→f8→f6→f4→f1 with vector directions defined in Figure 1d systematically generates new damage-free paths: detaching f7 in the arrow-indicated direction liberates spatial clearance for f6; harvesting f11 similarly unlocks space for f10, which

in turn creates clearance for f9. Proceeding sequentially, f8 becomes accessible after f9 is harvested, f4 and f1 become accessible after f6 is harvested. This cascading strategy transforms all blocked fruits (f1, f4, f6, f8, f9, f10, and f13) into harvestable targets.

Beyond maximizing damage-free harvesting success, efficiency improvements demand minimizing total travel distance during sequence execution. Thus, optimizing both the picking sequence and vector directions under spatial constraints becomes critical to enhance harvesting success rates and operational efficiency in clustered crops. Addressing this dual-objective problem -ensuring collision-free detachment while shortening path lengths- is pivotal to overcoming practical bottlenecks in robotic harvesting, accelerating its industrial adoption.

Definitions of adjacent and secondary adjacent fruits

The optimal damage-free vector detachment direction for a target fruit is primarily determined by its geometric relationships with surrounding fruits. Based on proximity, surrounding fruits that influence the viable detachment directions are categorized into adjacent fruits and secondary adjacent fruits, as illustrated in Figure 2. Specific definitions are as follows.

Adjacent fruits

Adjacent fruits are those in direct physical contact with the target fruit. A surrounding fruit is classified as adjacent if the center-to-center distance between it and the target fruit is $\leq R+r$ (where R is the radius of the target fruit, and r is the radius of the surrounding mushrooms). For instance, fruits f1 and f2 in Figure 2 are identified as adjacent fruits of target fruit f0.

Secondary adjacent fruits

In vector detachment operations, the fruit must be pushed or pulled along the detachment direction until a critical separation distance is reached for successful detachment. Thus, achieving reliable damage-free separation in dense clusters requires not only addressing adjacent fruits but also accounting for interference from fruits within the critical separation distance (d). For instance, in Figure 2, if only adjacent fruits are considered, target fruit f0 could theoretically be detached in direction D. However, during actual separation, f0 would collide with secondary adjacent fruits f3 and f4 before reaching the required separation distance, risking unintended displacement or damage. Hence, fruits outside the immediate adjacency zone but located within d_1 (the minimal clearance required for unobstructed detachment) from the target fruit's outer edge can still impede damage-free separation. This paper defines such fruits as secondary adjacent fruits, with d calculated as Eq. 1:

$$d=\sqrt{h^2+(r_0+\delta)^2} \quad \text{(Eq. 1)}$$

Where h, r_0 and δ denote the height of the target fruit, its radius, and the safety margin accounting for positioning uncertainties, sensor errors, or dynamic robotic movements, respectively.

Calculation of damage-free detachment direction set

All azimuth calculations in this section adopt a unified polar coordinate system: where horizontal right, counterclockwise rotation and 0-2 π continuous value denote the positive polar axis, positive angle direction and unique spatial direction definition, respectively, with no quadrant ambiguity.

In dense fruit harvesting, the damage-free detachment direction of the target fruit must simultaneously avoid geometric constraints imposed by adjacent fruits (direct contact) and secondary adjacent fruits (potential interference). The feasible solution set is the intersection of the constraint conditions from these two types of fruits. The specific calculation methods are as follows.

Damage-free detachment direction set calculation for target fruit and adjacent fruits

The core principle for calculating the damage-free detachment direction set of adjacent fruits lies in constraining the swing direction of the target fruit when harvested by a robotic arm. This ensures that the contact area between the target fruit and adjacent fruits does not expand as the harvesting path extends. If improper swing direction selection causes the overlapping area to increase, it will lead to a sharp rise in compressive stress between the fruits, potentially triggering rigid collisions between the robotic arm's end effector and adjacent fruits. Such collisions may result in fruit damage or mechanical jamming (Jia *et al.*, 2011).

The specific method for calculating the damage-free detachment directions of adjacent fruits is illustrated in Figure 3. Two intersecting circles O_0 (target fruit, radius R_0) and O_j (adjacent fruit, radius R_j) are considered. Critical tangent directions exist at the endpoints A and B of the common chord, which constrain the motion of O_0. For instance, when O_0 moves along the tangent at point A away from O_j to position O_0^{UP}, or along the tangent at point B to position O_0^{Down}, the common chord of the two circles remains a subset of the line segment AB. This ensures that the overlapping area of the two circles does not exceed the initial intersection region. Therefore, the angle range αj in the figure corresponds to the damage-free detachment direction range.

The tangent directions at the common chord endpoints A and B are symmetric about the line of centers (the line connecting O_j and O_0). Using the geometric relationship of the intersecting circles, the critical constraint angle α_j is derived as Eq. 2. Assuming the positive direction of the line of centers points from the adjacent fruit center O_j to the target fruit center O_0, with a center-to-center distance $||O_jO_0||$ and an angle θ_{j0} relative to the polar axis, the damage-free detachment direction set β_{Oj} is defined by Eq. 3.

$$\alpha_j=2\arccos\left(\frac{\|O_JO_O\|^2+R_0^2-R_J^2}{2\|O_JO_O\|R_0}\right) \quad \text{(Eq. 2)}$$

$$\beta_{oj}=\left[\theta_{jo}-\alpha_j/2,\theta_{jo}+\alpha_j/2\right] \quad \text{(Eq.3)}$$

Where β_{0j}, θ_{j0} and α_j denote the feasible range of damage-free detachment direction for the target fruit O_0 relative to the adjacent fruit O_j, the azimuth angle of the line of centers (from O_j to O_0) relative to the polar axis, and the critical constraint angle of damage-free detachment direction calculated by Eq. 2, respectively.

Damage-free detachment direction set calculation for target fruit and secondary adjacent fruits

In practical harvesting of quasi-spherical fruits, the damage-free picking space of the target fruit is constrained not only by its immediate adjacent fruits but also by interference from secondary adjacent fruits. By analogy to the movement direction of a pedestrian avoiding obstacles, the detachment direction of the target fruit P_0 treats secondary adjacent fruits P_j as obstacles during the vector-based separation process, and the blocking angles of each secondary adjacent fruit relative to the target fruit are calculated (Jia *et al*., 2011).

The specific method is illustrated in Figure 4. Draw the internal common tangents between the target fruit and the secondary adjacent fruit to obtain two tangent points A and B on the secondary adjacent fruit. Along the outward normal directions at points A and B, positions are defined at a distance equal to the fruit radius. For the target fruit P_0 (radius R_0) and secondary adjacent fruit P_j (radius R_j), with a center-to-center distance $||P_0P_j||$, the angle α_{0j} between the two internal common tangents is derived using the internal tangent theorem Eq. 4.

Assuming the positive direction of the line of centers is from the secondary adjacent fruit center P0 to the target fruit center Pj, with an orientation angle θj0 relative to the polar axis, the blocking angle range (non-viable damage-free detachment angles) is defined by Eq. 5. Consequently, the damage-free detachment angle range corresponds to the angles, as specified in Eq. 6.

$$\alpha_{oj}=2arcsin\left(\frac{R_0+R_J}{\|P_0P_J\|}\right) \quad \text{(Eq. 4)}$$

$$Q_{oj}=\left[\theta_{jo}-\alpha_{oj}/2,\theta_{jo}+\alpha_{oj}/2\right] \quad \text{(Eq. 5)}$$

$$\beta_{oj}=\left[2\Pi-\theta_{jo}+\alpha_{oj}/2,2\Pi-\theta_{jo}-\alpha_{oj}/2\right] \quad \text{(Eq. 6)}$$

Determination of optimal damage-free detachment direction

The damage-free detachment direction solution set B for the target fruit's secondary adjacent fruits is defined as the intersection of the solution sets of all secondary adjacent fruits and all immediate adjacent fruits, as shown in Eq. 7. If solution set B is ∅, it indicates no damage-free detachment directions exist within the secondary adjacent regions.

$$B=\bigcap_{j=1}^{h}\beta_{oj} \quad \text{(Eq.7)}$$

where h is the total number of immediate adjacent fruits and secondary adjacent fruits around the target fruit.

If no immediate adjacent fruits or secondary adjacent fruits exist around the target fruit, it signifies no surrounding obstacles, and any direction is viable for damage-free detachment. If solution set B=∅, the target fruit cannot be detached without damage. If B is non-empty, the optimal damage-free detachment direction df is determined by selecting the midpoint angle within the angular intervals of set B, as defined in Eq. 8:

$$d_f=\theta_{down}+\frac{\theta_{up}-\theta_{down}}{2} \quad \text{(Eq. 8)}$$

Where θ_{down} and θ_{up} are the lower bound and upper bound of the solution set, respectively.

Research on multi-objective optimization algorithm for dense fruit harvesting sequence based on vector detachment

Construction of multi-objective optimization model for harvesting sequence

As described above, the harvesting of densely clustered fruits needs to address two challenges: i) achieving a higher damage-free harvesting success rate; ii) obtaining a harvesting path with shorter length. Therefore, this paper simultaneously optimizes these two objectives.

Damage-free detachment failure rate

For the first challenge, as mentioned earlier, in the harvesting of densely clustered fruits using vector detachment, if a target fruit has no damage-free detachment direction during harvesting, it will lead to failure in damage-free harvesting. The smaller the number of target fruits without damage-free detachment directions, the higher the damage-free harvesting success rate. Therefore, the damage-free detachment failure rate function under vector detachment is adopted as one of the optimization objectives for harvesting sequence, defined as follows:

$f_1(seq)$: $p_{fail}=\frac{N_{fail}}{N}\times 100\%$ (Eq. 9)

where N Since altering the picking sequence changes the spatial distribution of adjacent Since the distribution of adjacent fruits around the target fruit changes with the picking order, thereby altering the feasibility of its lossless separation, the calculated results for the same dense fruit cluster will differ under different picking sequences. The specific calculation method is as follows: For a dense fruit cluster containing N mature fruits and any given picking sequence, Iteratively compute the solution set C for each target fruit according to the method for determining lossless vector separation directions described in the previous section.. If the solution set C is empty, it indicates that the target fruit has no viable lossless vector separation direction, and N_{fail} is incremented by 1. This process is repeated across the entire picking sequence.

Path length of picking sequence

The second problem is a common path optimization issue, where the total path length of the picking sequence is typically chosen as the optimization objective. The calculation is defined as follows:

$$f_2(seq) : dist_{sum}=\sum_{i=1}^{N-1}\sqrt{(x_{i+1}-x_i)^2+(y_{i+1}-y_i)^2} \quad \text{(Eq. 10)}$$

Where: x and y are the horizontal and vertical coordinates of mature fruits respectively.

Establish multi-objective optimization model

In summary, the multi-objective optimization model for picking order of dense fruit sets in this paper takes the minimum failure rate of lossless separation of fruits to be picked under vector separation and the shortest picking path length as the optimization objectives, as shown below:

$$MinF(seq)=[f_1(seq),f_2(seq)] \quad \text{(Eq. 11)}$$

Objective function preprocessing

To eliminate the significant dimensional and magnitude discrepancies between the failure rate objective f_1 and path length objective f_2, a min-max normalization strategy is adopted for objective function preprocessing. For each objective in the current population, the normalized value is calculated as:

$$f'_k(seq)=\frac{f_k(seq)-f_{k,\min}}{f_{k,\max}-f_{k,\min}+\varepsilon},\ k=1,2 \quad \text{(Eq. 12)}$$

where $f_{k,\min}$ and $f_{k,\max}$ denote the minimum and maximum values of the k-th objective in the

current population, respectively, and ε=10−10 is a small constant to avoid division by zero. This linear scaling maps both objectives to the range of [0,1], and the normalized values are used for all subsequent evolutionary operations (including fast non-dominated sorting, crowding distance calculation, and elite selection) to ensure equal contribution of the two objectives.

Multi-objective optimization algorithm for picking order of dense fruit set based on improved NSGA-II

Multi-objective optimization algorithm mainly includes weighted coefficient method (Behnamian *et al*., 2021), multi-objective genetic algorithm and multi-objective particle swarm optimization algorithm, *etc*. (Cao *et al*., 2021). NSGA-II is widely used in engineering practice as a second generation improved algorithm of non-dominated sorting genetic algorithm (NSGA) (Pereira *et al*., 2022). In particular, the NSGA-II algorithm showed superior performance in combination optimization problems such as sequence planning, vehicle routing problem and allocation problems (Verma *et al*., 2021). Shuai *et al*. (2019) have improved the crossover and mutation operators in NSGA-II and used the improved NSGA-II to optimize the multi-objective when solving the optimization of the difference between the total journey distance and the longest and shortest trip in the multi-traveler problem. In order to obtain a shorter, safer and smoother robot path in a static known environment, Xue *et al*. (2018) optimize the individual path by using short circuit, security and smooth operation, and solve the multi-target path planning problem of mobile robot by combining with NSGA-II algorithm.

Therefore, NSGA-II algorithm is applied to optimize the order of picking of dense fruits requiring vector separation in this paper. However, although the NSGA-II algorithm has been further enhanced in terms of optimization ability by using non-dominant sorting, crowding distance, and elite strategy, it still requires larger population size and more evolutionary generations to optimize for appropriate results to solve the multi-objective picking sequence optimization problem in this paper by using the traditional NSGA-II (Laszczyk *et al*., 2019), and the overall optimization performance by NGSA-II is not ideal. So, we further improved the NSGA-II algorithm by using PSO single-objective optimization solution as extreme point to inject into initialization population and adding elite strategy individual screening to improve the initial population quality so as to accelerate the convergence speed of the algorithm, by adopting a phased adjusted cross-probability control method while improving the algorithm's local search capability by 2-opt, and by using circular sorting algorithm to improve the uniformity and diversity of Pareto front solution. The improved algorithm is called I-NSGA-II

in this paper, and its specific process is shown in Figure 5.

The initialization of population

The initialization of a population is mainly based on the problem to identify individual coding method and its population size. The initial population has great influence on the convergence of the algorithm. In order to further accelerate the convergence of the algorithm and improve its operation efficiency, the initial population extremum injection is used here.

As mentioned earlier, the harvesting sequence planning for dense clusters prioritizes two objectives: minimizing the failure rate of lossless separation and optimizing harvesting path length. Given the limited spatial constraints around fruits and relatively simple fruit distribution patterns, resolving the issue of fruit separation without lossless direction—which reduces the complexity of failure rate optimization— proves more manageable than optimizing harvesting path length. single-objective optimization results for dense clusters in Figure 6 demonstrate that: i) the path length optimization method targeting shortest harvesting paths achieved 1027mm with a 24% failure rate reduction; ii) the failure rate minimization approach reduced failure rates to 8% but resulted in a harvesting path length of 2855 mm, 2.8 times longer than the optimal path. This demonstrates that constrained optimization simultaneously reduces separation failure rates while maintaining harvesting efficiency due to limited fruit space and simple surrounding conditions. Conversely, failure rate optimization without path length constraints often leads to excessive path length waste, failing to enhance both success rates and harvesting efficiency. Additionally, our study found that individuals with lower failure rates tend to emerge more frequently in initial populations, whereas those with superior harvesting path lengths are less likely to appear. Therefore, even when individuals with lower failure rates of lossless separation are injected into the initial population as extreme points, it remains challenging to achieve significant leading advantages. This motivates our choice to optimize path length in harvesting routes as the primary objective during extreme point injection. The particle swarm optimization (PSO) algorithm demonstrates superior convergence efficiency compared to other single-objective evolutionary algorithms when addressing path length optimization problems (Panda, 2018). Consequently, we employ the PSO algorithm to optimize harvesting route lengths for fruit picking, then inject the optimized solutions into the initial population to enhance algorithmic convergence.

Quick non-dominant sorting and crowding distance calculation

The crowding distance of individuals in the same non-dominated front is calculated based on

the normalized objective values, which eliminates the magnitude bias between the two objectives and ensures unbiased diversity maintenance of the population.

Quick non-dominant sorting: the dominant relationship between individuals was determined by the individual fitness value, and different levels are distributed to individuals.

Crowding distance calculation: once the sorting operation is complete, the crowding distance for the same level of individuals is calculated. In the traditional NSGA-II algorithm, the crowding distance of all individuals at the same rank is calculated by using a crowding distance comparison operator, and then all individuals with a certain number of small congestion distances are deleted at once. This retention of individuals may result in a sparse and uncertain distribution of Pareto front solutions, which does not guarantee uniformity of solutions and may have some impact on the diversity of solutions as well. Therefore, this paper uses circular crowding sorting algorithm instead of traditional crowding distance comparison operator to maintain the uniformity and diversity of the Pareto front solutions (Liu *et al*., 2021).

Initial population quality enhancement: in order to improve the optimization efficiency of the algorithm, a population quality enhancement operation was carried out on the initial population, and $2\times p_{size}$ individuals in random initial temporary population were selected as the initial population by an elite strategy, and then from which p_{size} individuals were selected as the initial population. Before screening, the corresponding nondestructive separation failure rate p_{fail} and the picking path length $dist_{sum}$ are calculated for each individual in the temporary population by Eqs. 9 and 10, and then assign an i_{rank} level to each solution in the population by using the non-dominant sorting based on the concept of dominance. The superiority of different individuals in the same class is then compared by the crowding distance shown in Eq. 12 to select the superior individual.

$$i_{dist}= \sum_{k=1}^{m} \frac{z_k(i+1)-z_k(i-1)}{z_k^{max}-z_k^{min}},\ 2\le i\le q-1 \qquad \text{(Eq. 13)}$$

where: m is the number of objective functions, $z_k(i)$ is the kth objective function value for the ith solution, z_k^{max}, z_k^{min} are the maximum and minimum values on the objective function, respectively, q is the number of solutions at the specified level.

Selection, crossover and mutation

Tournament selection, two-point crossover and one-point mutation were used here. In order to improve the global search capability of the algorithm, phased adjustment of crossover probability is adopted. And the 2-opt algorithm is improved to increase the local search ability

and accelerate convergence.

Phased adjustment of crossover probability: the function of crossover focuses on the global search of the algorithm and the size of crossover probability determines the diversity of population. Different stages of evolution require different population diversity. In the early stages of evolution, as many diverse individuals as possible are often needed to help find excellent solutions. In the later stages of evolution, algorithms converge on optimal solutions, which require less crossover probability. In this study, the crossover was operated by a two-point crossover. The crossover probability was controlled by phased adjustment (Wang, 2018), which divides the entire evolutionary process into early, mid, and late stages of evolution, with the algorithm adapting the crossover probabilities to the evolutionary stage and adjusting the crossover probability rules in stages as follows:

$$p_c=\begin{cases}\frac{0.25(T_1-t)}{T_1}+0.75, & t\in[0,T_1]\\ \frac{0.25(T_1-t)}{T_2-T_1}+0.5, & t\in(T_1,T_2]\\ \frac{0.5(T-t)}{(T-T_2)(1-\beta)}+0.5\beta, & t\in(T_2,T]\end{cases} \quad \text{(Eq. 14)}$$

where, T is the maximum number of evolutionary generations, $T_1=\alpha T$， $T_2=(1-\alpha)T$； β is the adjustment factor for the crossover probability in late evolution, $\beta\in(0,1]$, which is set to ensure that the crossover probability asymptotically approaches a value that is not zero in late evolution. In this study, α was taken as 0.382 and β as 0.4.

Mutational operator improvement: the role of the Mutation focuses on local search, and a single point mutation is chosen for the mutation operation in this study. In order to further accelerate convergence and enhance the local search capability of the algorithm, a 2-opt algorithm is added to the mutation to enable the adjustment of the mutated individuals.

New parent population generation

Combining parent and offspring populations, and the new generation is determined by elite strategies.

When the crossover and mutation probabilities are not 1, the NSGA-II algorithm, after evolving to a specified number of generations, the diversity of solutions decreases dramatically, and the entire solution space of Pareto contains only a small number of solutions. De Moraes and Coelho (2022) show that for multi-objective optimization problem, due to certain probability that some not to perform genetic operations, a large number of repeated solutions will appear in the temporary population after the parent and child populations are merged. Therefore, in order to improve the diversity of solutions, this research adds a duplicate individual control

strategy (Zhang *et al*., 2022) to the traditional algorithm to remove duplicate individuals from the temporary population. The specific steps for controlling duplicate individuals strategy are as follows.

i) Remove duplicate individuals in the combined population R_t of parental P_t and offspring Q_t.

ii) Judging whether the number of remaining individuals in the de-duplicated population R_t is smaller than the population size N (100) of P_t, if it is smaller, continue tournament selection, crossover, mutation and merging of populations and return to i). Otherwise calculate $p_{fail}$and $dist_{sum}$, the objective function values for the individuals in the merged population after de-duplication. Perform fast non-dominated sorting and crowding degree calculation for individuals in population R_t. And the final temporary population R_t is obtained after dereplication.

Optimal solution selection

The linear programming technique for multidimensional analysis of preference (LINMAP) is used as the decision method for the optimal solution, and a solution from the Pareto front solution is selected as the final output.

Theoretical convergence and computational complexity analysis

The proposed improvements (PSO extremum injection, cyclic crowding sorting, 2-opt local search, and staged crossover probability) form a synergistic closed-loop optimization framework, not a simple superposition. Based on Markov chain theory, the elitism mechanism ensures monotonic convergence, the staged genetic operators guarantee ergodicity, and the cyclic crowding sorting maintains population diversity. Thus, I-NSGA-II converges to the global Pareto optimal set with probability 1. The overall computational complexity is O (GMN^2), the same order as standard NSGA-II, with affordable overhead from the improvement modules.

Results

Experimental data acquisition and preprocessing

All experimental data were collected from a commercial *Agaricus bisporus* planting base in Shanghai, China. Industrial cameras captured in-situ growth images, and a YOLOv8 instance segmentation model extracted mushroom features (X,Y,R,H). After manual verification and

denoising, six representative distribution patterns were screened from the field dataset for algorithm validation. No artificially generated virtual data were used.

Experimental results of improved picking sequence planning algorithm (I-NSGA-II)

The growth of fruits is random, and their clustering degree, distribution uniformity, and the extent to which individual fruits are surrounded by others exhibit complex diversity. Based on field observations, this study designed six typical dense fruit growth distribution patterns as experimental data to validate the effectiveness of the proposed I-NSGA-II algorithm. The key parameters of the I-NSGA-II algorithm in this experiment are as follows: the maximum number of iterations is set to 80, the population size is 60, and the tournament size is 4. To verify the adaptability of the algorithm in real agricultural scenarios, picking strategies generated by MO-PSO, NSGA-II, and the improved I-NSGA-II algorithm were compared. The differences in path optimization efficiency and occlusion resolution capability among these algorithms intuitively reflect their comprehensive performance under multi-constrained conditions.

Experiment 1: dense cluster of fruiting bodies containing only mature fruiting bodies

As shown in Figure 7a, all fruiting bodies in the dense cluster are mature and require harvesting, totaling 13 mature fruiting bodies. Among them, 5 initial "fully enclosed" state fruiting bodies (f3, f6, f5, f9, f10) are present, accounting for 38.4% of the cluster. The harvesting strategies optimized by the multi-objective optimization algorithms MO-PSO, NSGA-II, and I-NSGA-II are illustrated in Figure 7 b-d, respectively.

This experiment conducted a multi-algorithm comparative analysis targeting the case illustrated in Figure 7a. The specific optimization results are summarized in Table 1. The experimental results demonstrate that: i) The single-objective GA algorithm and the dual-objective optimization algorithms NSGA-II and I-NSGA-II achieved Pclosed = 0%, successfully converting all fully enclosed fruits into semi-enclosed states through harvesting sequence reconstruction. In contrast, the MO-PSO algorithm underperformed on this metric, leaving 1 fully enclosed fruiting body unprocessed, indicating a significant difference in its optimization capability for damage-free harvesting success. ii)The dual-objective optimization algorithms (MO-PSO, NSGA-II, and I-NSGA-II) reduced the average harvesting path length by 40% compared to the single-objective GA algorithm. Notably, the proposed improved I-NSGA-II algorithm exhibited the best performance. After iterative convergence, it achieved a minimum total path length (Dsum) of 1390 mm, which is 7.5% lower than that of the traditional NSGA-II algorithm.

Experiment 2: dense cluster of fruiting bodies with both mature and immature fruiting bodies

This experiment builds a test case based on the high-density mixed-growth distribution pattern of an actual fruiting cluster, as shown in Figure 8a. The scenario contains 28 fruiting bodies (17 mature fruits and 11 immature fruits). Among the mature fruiting bodies, 9 are in a "fully enclosed" state (f5–f7, f10–f12, f14, f16–f17), accounting for 52.94% of the mature group. This cluster exhibits heterogeneous distribution characteristics of mature and immature fruits. Compared to the arrangement in Experiment 1, this instance presents higher optimization complexity in terms of spatial occlusion correlations, target harvesting priorities, and path accessibility. The harvesting strategies optimized by the multi-objective algorithms MO-PSO, NSGA-II, and I-NSGA-II are shown in Figure 8 b-d, respectively.

This experiment conducted a comparative analysis of multiple algorithms based on the mixed mature/immature mushroom cluster in Figure 8a. The experimental data from Table 2 show the following results: i) the single-objective GA algorithm and the proposed I-NSGA-II algorithm reduced the harvesting failure rate to Pclosed = 5.8%, significantly outperforming NSGA-II (11.7%) and MO-PSO (23.5%); notably, the mature fruiting body f16 is fully enclosed by immature mushrooms, leaving no operational space for damage-free separation; this results in an unoptimizable theoretical lower limit for failure rates. ii) The dual-objective optimization algorithms (MO-PSO, NSGA-II, and I-NSGA-II) achieved an average 50% reduction in path length compared to the single-objective GA approach. The proposed improved I-NSGA-II algorithm demonstrated exceptional performance, generating a global optimal total path length (Dsum) of 1998 mm after convergence - 5.4% shorter than the 2112 mm path produced by traditional NSGA-II. The experimental results confirm that the proposed algorithm effectively maintains low-damage harvesting characteristics while generating superior harvesting paths for dense mushroom clusters containing mixed mature/immature fruiting bodies.

Experiment 3: highly aggregated fruiting body cluster

To further evaluate the optimization capability of the proposed algorithm for more complex fruit aggregation scenarios, this experiment tests a denser cluster (Figure 9a) comprising 38 fruiting bodies (24 mature and 14 immature). Among the mature fruiting bodies, 15 are in a "fully enclosed" state (f3, f7, f8, f9, f10, f11, f13, f14, f15, f16, f17, f19, f20, f21, f22), accounting for 62.5% of the mature group. Compared to Experiment 2, this cluster exhibits significantly higher aggregation density, posing substantial optimization challenges in harvesting sequence planning. The harvesting strategies optimized by the multi-objective

algorithms MO-PSO, NSGA-II, and I-NSGA-II are illustrated in Figure 9 b-d, respectively.

This experiment conducted a multi-algorithm comparative study based on the highly aggregated cluster shown in Figure 9a. The experimental data in Table 3 reveal the following: i) the proposed I-NSGA-II algorithm reduced the harvesting failure rate to Pclosed=16.6%, significantly outperforming the single-objective GA algorithm (20%), NSGA-II (20.8%), and MO-PSO (29.1%); ii) the dual-objective optimization algorithms (MO-PSO, NSGA-II, and I-NSGA-II) achieved an average 50% reduction in path length compared to the single-objective GA method. The improved I-NSGA-II algorithm demonstrated exceptional performance, yielding a global optimal total path length (Dsum) of 2722 mm after convergence. This result is 20.2% shorter than the 3414 mm path generated by the traditional NSGA-II algorithm and 17.8% shorter than the MO-PSO algorithm. The proposed I-NSGA-II algorithm exhibits outstanding performance in handling highly aggregated clusters of mixed mature/immature fruiting bodies, balancing both low failure rates and optimized harvesting efficiency.

In summary, the I-NSGA-II multi-objective optimization algorithm demonstrates robust adaptability to clustered fruits of varying aggregation densities, achieving the following: i) it successfully harvests all mature fruiting bodies in a damage-free manner except those in irreparable "fully enclosed" states, effectively minimizing the average damage-free harvesting failure rate; ii) the algorithm reduces the total harvesting path length to 55% of the single-objective optimization results on average. This dual achievement significantly lowers both the failure rate and operational time, enabling high-efficiency, low-damage harvesting of densely clustered fruits. The I-NSGA-II algorithm offers a pioneering solution for balancing precision and efficiency in complex agricultural harvesting scenarios, demonstrating superior performance in handling clusters with heterogeneous maturity and aggregation states.

Experiment 4: comparison of the optimization performance of the improved multi-objective optimization algorithm with other multi-objective algorithms

The optimization performance of the improved algorithm in this paper is compared with that of the traditional NSGA-II and MO-PSO algorithms.

Evaluation indicators

The three evaluation indicators below are selected to evaluate optimization performance of the multi-objective optimization algorithms mentioned in this paper.

Euclidean distance (ED): the ED is a multi-objective evaluation indicator for measuring the convergence of an algorithm (Laszczyk and Myszkowski, 2019). Convergence is evaluated by

using the average distance between each point on the approximate Pareto front and the ideal point, which includes the best value for all objectives. The smaller the value of this evaluation indicator, the better the convergence, and it is defined as follows:

$$d_m=\sum_{k=1}^{M}\left(\frac{f_k(m)-f_k(perfect)}{f_k^{max}-f_k^{min}}\right)^2 \quad \text{(Eq. 15)}$$

$$ED(PF)=\min_{i\in|PF|} d_m \quad \text{(Eq. 16)}$$

ehere: PF is the Pareto front, and d_m is the Euclidean distance from the m-th point in the Pareto front solution to the ideal point.

<u>*Hypervolume (HV):*</u> the HV measures the space dominated by an individual (Acciarini *et al*., 2020) and can evaluate both the convergence and diversity of the non-dominated solution sets obtained by the algorithm. It is a comprehensive evaluation indicator and the larger the value, the better the convergence and diversity of the algorithm. It is defined as follows:

$$HV(PF)=\Lambda\left(\cup_{S\in PF}\{S'|S\prec S'\prec S^{nadir}\}\right) \quad \text{(Eq. 17)}$$

where PF represents the approximate Pareto front, S is the point in PF, and S^{nadir} is the non-ideal point.

<u>*Spacing (SP)*</u>: the SP is a diversity indicator that measures only the uniformity of the distribution of the solution set, and a smaller SP value represents a better distribution of the solution set S. It is defined as follows:

$$SP(S)=\sqrt{\sum_{i=1}^{|S|}\frac{(d_i-\bar{d})^2}{|S|-1}} \quad \text{(Eq. 18)}$$

$$d_i=\min_{x^j\in S,x^i\neq x^j}\sum_{k=1}^{m}|F_k(x^i)-F_k(x^j)| \quad \text{(Eq. 19)}$$

where d_i is the distance between the two closest solutions.

Performance comparison of different multi-objective optimization algorithms

In this section, the proposed I-NSGA-II algorithm, the traditional NSGA-II algorithm, and MO-PSO algorithm were applied to conduct multi-objective harvesting sequence optimization experiments on six fruit distribution scenarios (labeled A-F in Figure 10) with varying aggregation densities. The optimization results are summarized in Figure 11, which presents the averages of the ED, HV, and SP evaluation metrics obtained after six independent runs of

each algorithm on different fruit distributions.

Firstly, the comparison of the ED values of each algorithm under each distribution is shown in Figure 11a. The blue, green and yellow polylines represent the ED values of I-NSGA-II, MO-PSO and traditional NSGA-II algorithm respectively. The non-dominated solutions obtained by I-NSGA-II all achieved the smallest ED values, which indicates that I-NSGA-II has the best convergence among the three algorithms. Next, I-NSGA-II also outperforms the other two algorithms in terms of HV, with a significantly higher HV value, which is more than 2.6 times that of the other two algorithms, indicating that I-NSGA-II has the best comprehensiveness, i.e., diversity and convergence of solutions, as shown in Figure 11b. Finally, the I-NSGA-II does not consistently rank first among the three algorithms in terms of the SP metric. This outcome can likely be attributed to the application of the cyclic crowding distance algorithm. The cyclic crowding distance algorithm addresses the shortcomings of the traditional NSGA-II in the crowding distance comparison operator, enabling the algorithm to explore regions with larger gaps in the Pareto front more thoroughly. For the uniformity evaluation metric SP, this approach to maintaining solution diversity can lead to significant fluctuations in the SP metric. Therefore, it is reasonable that the SP value of I-NSGA-II does not always occupy the top position among the three algorithms. This does not undermine the superiority of the proposed algorithm in this study. As evidenced by the other two evaluation metrics, ED and HV, the I-NSGA-II algorithm demonstrates clear advantages in terms of convergence and the preservation of solution diversity.

To compare the optimization capabilities of algorithms more intuitively, Figure 12 displays the non-dominated frontier solution sets for all test instances obtained by each of the three algorithms. As can be seen from these diagrams, the solution set obtained by the I-NSGA-II algorithm is closer to the ideal point than the other two algorithms. Therefore, it has advantages in convergence and diversity.

Discussion

For the optimal damage-free separation direction of target fruits, as seen from the trajectory optimization experimental results for fruit distributions with different aggregation densities in Section 5, whether in simple-distribution fruit clusters or complex-distribution ones, all target fruits can obtain optimal damage-free separation directions through the graph theory-based method proposed in this study. For the damage-free harvesting sequence optimization problem in dense fruit clusters, observations from Experiments 1, 2, and 3 show: the single-objective optimization GA algorithm (optimizing only damage-free separation failure rate) achieved a

damage-free separation failure rate comparable to the dual-objective optimized I-NSGA-II algorithm, but the path lengths optimized by I-NSGA-II were shortened by 39.5%, 52.8%, and 55.6% respectively compared to GA. This demonstrates that compared to single-objective optimization, the multi-objective optimization algorithm not only maintains equivalent optimization effectiveness on damage-free separation failure rate but also significantly reduces harvesting path lengths. The multi-objective algorithm optimizing both minimal damage-free failure rate and shortest harvesting path outperforms the single-objective approach, achieving high-efficiency low-damage harvesting for dense fruits.

In Experiment 2, where clusters contained unripe fruits excluded from harvesting, the optimized damage-free failure rate reached 5.8% (failing to attain the theoretical minimum 0%) because in highly aggregated distributions, a small subset of mature fruits were entirely surrounded by unripe fruits, leaving no feasible damage-free separation direction. As unripe fruits remain unpicked, no path optimization can resolve such cases, making 0% failure theoretically unachievable. Thus, I-NSGA-II already optimized the failure rate to its ideal theoretical limit. This confirms the algorithm's excellent optimization capability even under complex distributions.

In Experiment 3 (extremely dense clusters), I-NSGA-II reduced the failure rate to 16.6%, 3.4% lower than GA's 20%. As aggregation density increases, all algorithms exhibit declining performance, but single-objective methods degrade more severely. The cyclic crowding strategy in I-NSGA-II enhances solution diversity compared to traditional NSGA-II and GA, enabling better Pareto solutions, while phased crossover probability adjustments and the 2-opt algorithm further strengthen global/local search capabilities. Therefore, for complex problems, I-NSGA-II's improvements in diversity, search ability, and convergence significantly enhance optimization performance over traditional algorithms, with advantages magnified as problem complexity grows. Though I-NSGA-II's optimization slightly declines with increasing fruit aggregation, its margin of decline remains small, still yielding superior solutions. This validates the algorithm's strong applicability for dense fruit harvesting sequence planning.

Conclusions

The purpose of this work is to enable fruit-picking robots to avoid collision damage between fruits and achieve high-efficiency harvesting of densely clustered fruits. In this study, a multi-objective planning method for picking sequences of dense fruits requiring vector separation was proposed and experimentally validated. The results indicate that:

i) The non-destructive vector separation optimal direction determination method, designed in

this study based on the geometric constraint model of critical tangent directions, is capable of effectively calculating the optimal separation direction for target fruits surrounded by others. This approach significantly mitigates the risk of fruit damage caused by collisions during the harvesting process.

ii) The proposed multi-objective optimization model, which aims to minimize vector picking failure rate and shorten picking path length, combined with the I-NSGA-II algorithm for planning dense fruit picking sequences, significantly improves the success rate of damage-free fruit harvesting—nearly achieving an ideal 100% success rate. Simultaneously, it reduces the average picking path length to 50% of single-objective optimization results, substantially enhancing picking efficiency. The comprehensive optimization effect far surpasses single-objective methods, particularly for increasingly complex and dense fruit distributions. The core framework of this method has the potential to be extended to 3D non-planar dense fruit harvesting scenarios by upgrading the geometric constraint model.

iii) An improved NSGA-II algorithm (I-NSGA-II) was developed. Building upon traditional NSGA-II, this algorithm enhances convergence speed through PSO-derived extremum point injection for population initialization and elite strategy-based individual screening. It employs a phased adjustment of crossover probability and 2-opt operations to strengthen global/local search capabilities, along with cyclic crowding distance sorting to improve Pareto front uniformity and diversity. The I-NSGA-II achieves an HV value 2.6 times higher than traditional NSGA-II and MO-PSO algorithms, effectively overcoming limitations in solving sequence optimization problems that typically require larger populations and more generations. The improvements include extremum point injection, phased crossover probability adjustment, cyclic crowding sorting, and deduplication operations.

In conclusion, the proposed method demonstrates superior damage-free harvesting performance for densely clustered fruits across various distribution patterns, particularly suited for vector separation-based picking sequence planning for quasi-planar growing button mushrooms. It should be noted that this study currently focuses on the quasi-planar clustered growth scenario of button mushrooms, and the plane projection-based model has not been specifically optimized for 3D non-planar dense growth crops such as kiwifruit and tomato, which is the main limitation of the current method. However, the core collision-free geometric constraint model and multi-objective sequence optimization framework proposed in this study have clear scalability for 3D spatial scenarios. In subsequent research, we will carry out targeted optimization for 3D non-planar dense growth crops, by extending the 2D planar geometric constraint model to a 3D spatial model, to solve the problem of difficulty in finding a suitable plane projection for side

harvesting in 3D scenarios. In addition, due to its reliance on a single separation strategy, some mature fruits lacking viable separation directions remain unharvested, resulting in minor picking omissions. Future work may integrate hybrid separation methods to optimize picking sequences and further reduce omission rates.

References

Acciarini G, Izzo D, Mooij E, 2020. MHACO: a multi-objective hypervolume-based ant colony optimizer for space trajectory optimization. Proc. IEEE Congr. Evolutionary Computation (CEC), Glasgow; pp. 1-8.

Behnamian J, Dezfooli SM, Asgari H, 2021. A scatter search algorithm with a novel solution representation for flexible open shop scheduling: a multi-objective optimization. J Supercomput 177:13115-13138.

Bu L, Hu G, Chen C, Sugirbay A, Chen J, 2020. Experimental and simulation analysis of optimum picking patterns for robotic apple harvesting. Sci Hortic 261:108937.

Cao X, Yan H, Huang Z, Ai S, Xu Y, Fu R, Zou X, 2021. A multi-objective particle swarm optimization for trajectory planning of fruit picking manipulator. Agronomy 11:2286.

Chen Z, Lei X, Yuan Q, Qi Y, Ma Z, Qian S, Lyu X, 2024. Key technologies for autonomous fruit-and vegetable-picking robots: A review. Agronomy 14: 2233.

Dai N, Fang J, Yuan J, Liu Z, 2024. 3MSP2: Sequential picking planning for multi-fruit congregated tomato harvesting in multi-clusters environment based on multi-views. Comput Electron Agric 225:109303.

de Moraes MB, Coelho GP, 2022. A diversity preservation method for expensive multi-objective combinatorial optimization problems using novel-first tabu search and MOEA/D. Expert Syst Appl 202:117251.

Gong L, Wang W, Wang T, Liu C, 2022. Robotic harvesting of the occluded fruits with a precise shape and position reconstruction approach. J Field Robot 9:69-84.

Hu X, Pan Z, Lv S, 2019. Picking path optimization of agaricus bisporus picking robot. Math Probl Eng 7:1-16.

Huang W, Miao Z, Wu T, Guo Z, Han W, Li T, 2024. Design of and experiment with a dual-arm apple harvesting robot system. Horticulturae 10:1268.

Jia HF, Chen B, Li GW, Zhang JS, 2011. Collision avoidance method in pedestrian simulation based on blockade-angle. J Jilin Univ Eng Technol Ed 41:6.

Kurtser P, Edan Y, 2020. Planning the sequence of tasks for harvesting robots. Robot Auton Syst 131:103591.

Laszczyk M, Myszkowski PB, 2019. Survey of quality measures for multi-objective optimization. Construction of complementary set of multi-objective quality measures. Swarm Evol Comput 48:109-133.

Lehnert C, McCool C, Sa I, Perez T, 2018. A sweet pepper harvesting robot for protected cropping environments. arXiv:1810.11920.

Liu C, Gong L, Yuan J, Li Y, 2022. Current status and development trends of agricultural robots. Trans Chin Soc Agric Mach 53:1-22.

Liu T, Yuan Q, Wang L, Wang Y, Zhang N, 2021. Multi-objective optimization for oil-gas production process based on compensation model of comprehensive energy consumption using improved evolutionary algorithm. Energy Explor Exploit 39:273-298.

Matache MG, Cristea R, Ionescu A, Epure M, 2024. Robots for harvesting solanaceae vegetables–review. Ann Fac Eng Hunedoara 22:39-47.

Ning Z, Luo L, Ding XM, Dong Z, Yang B, Cai J, et al., 2022. Recognition of sweet peppers and planning the robotic picking sequence in high-density orchards. Comput Electron Agric 196:106878.
Panda M, 2018. Performance comparison of genetic algorithm, particle swarm optimization and simulated annealing applied to TSP. Int J Appl Eng Res 13:6808-6816.
Pereira JLJ, Oliver GA, Francisco MB, Cunha SS Jr, Ferreira Gomes G, 2022. A review of multi-objective optimization: methods and algorithms in mechanical engineering problems. Arch Comput Methods Eng 29:2285-2308.
Shuai Y, Yunfeng S, Kai Z, 2019. An effective method for solving multiple travelling salesman problem based on NSGA-II. Syst Sci Control Eng 7:108-116.
Silwal A, Davidson JR, Karkee M, Mo C, Zhang Q, Lewis K, 2017. Design, integration, and field evaluation of a robotic apple harvester. J Field Robot 34:1140-1159.
Tang Z, Xu L, Xie H, 2020. Picking trajectory planning of citrus based on improved immune algorithm and binocular vision. Proc. IEEE Int. Conf. Artificial Intelligence and Computer Applications, Dalian; pp. 6-10.
Verma S, Pant M, Snasel V, 2021. A comprehensive review on NSGA-II for multi-objective combinatorial optimization problems. IEEE Access 9:57757-57791.
Wang BX, Wang SA, Yu DH, 2016. Fruit cluster recognition and picking sequence planning based on selective attention. Trans Chin Soc Agric Mach 47:1-7.
Wang G, Zhao Y, Wang Z, Zhang Y, 2022a. Tea picking path planning based on ant colony algorithm. Proc. 41st Chinese Control Conference (CCC), Hefei; pp. 1945-1950.
Wang HY, 2018. Multi-objective optimization algorithm and its application in path planning of mobile robot. Master's Thesis, Lanzhou University of Technology.
Wang ZH, Xun Y, Wang YK, Yang QH, 2022b. Review of smart robots for fruit and vegetable picking in agriculture. Int J Agric Biol Eng 15:33-54.
Xiong Y, Ge Y, Grimstad L, From PJ, 2020. An autonomous strawberry-harvesting robot: Design, development, integration, and field evaluation. J Field Robot 37:202-224.
Xiong Y, Peng C, Grimstad L, From PJ, Isler V, 2019. Development and field evaluation of a strawberry harvesting robot with a cable-driven gripper. Comput Electron Agric 157:392-402.
Xue Y, 2018. Mobile robot path planning with a non-dominated sorting genetic algorithm. Appl Sci 8:2253.
Yang S, Jia B, Yu T, Yuan J, 2022. Research on multiobjective optimization algorithm for cooperative harvesting trajectory optimization of an intelligent multiarm straw-rotting fungus harvesting robot. Agriculture 12:986.
Zhang SJ, Du HT, Hou TT, 2022. Improved NSGA2 algorithm to solve the multi-objective dual-resource flexible workshop scheduling problem. Proc. IEEE Int. Conf. Artificial Intelligence and Computer Applications, Dalian; pp. 771-778.

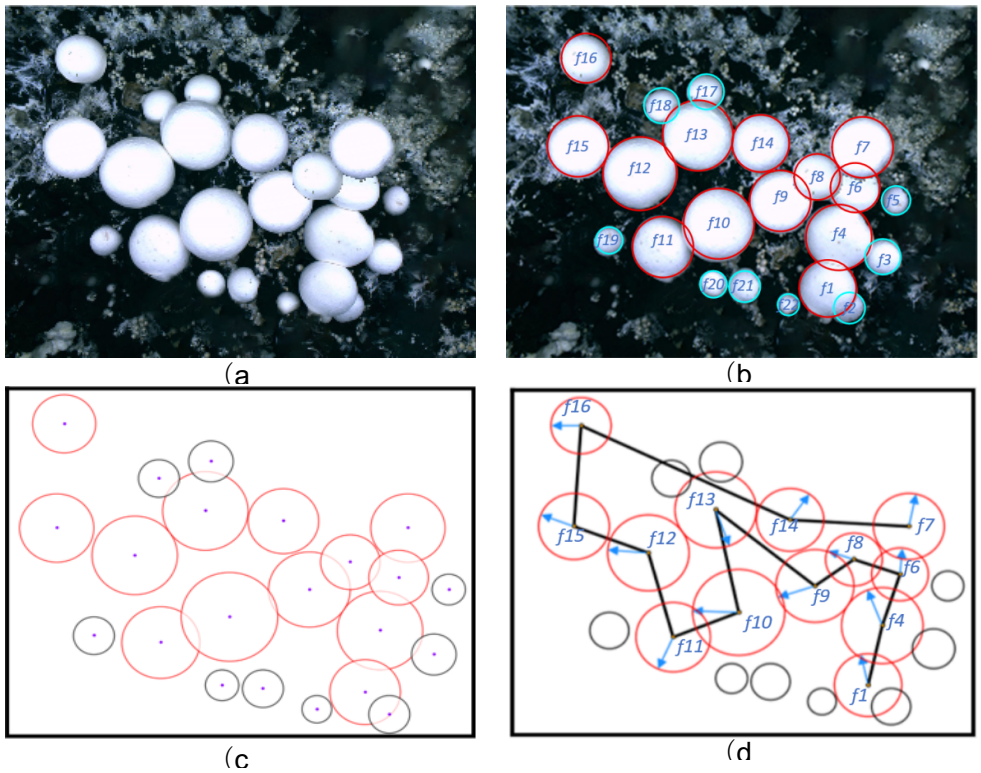

Figure 1. The optimal determination schematic for lossless vector separation direction.

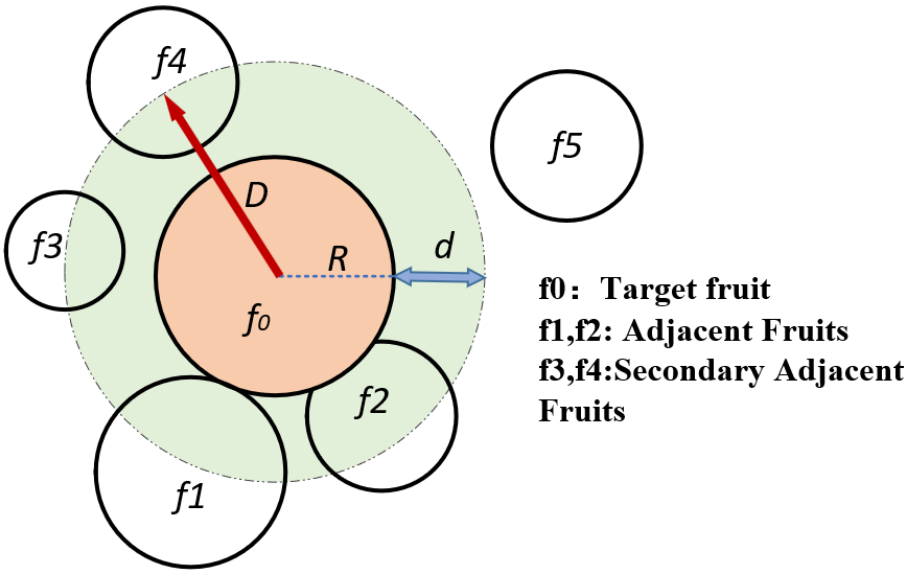

Figure 2. Spatial relationship of target fruit with surrounding fruits.

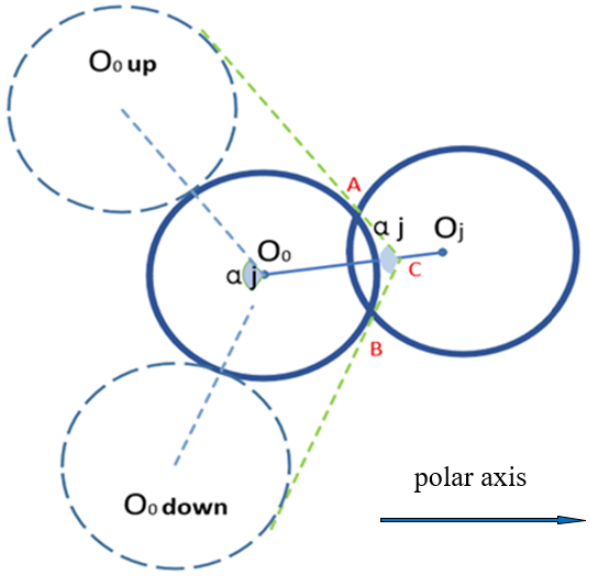

Figure 3. Schematic diagram of direction of lossless fruit separation in adjacent regions.

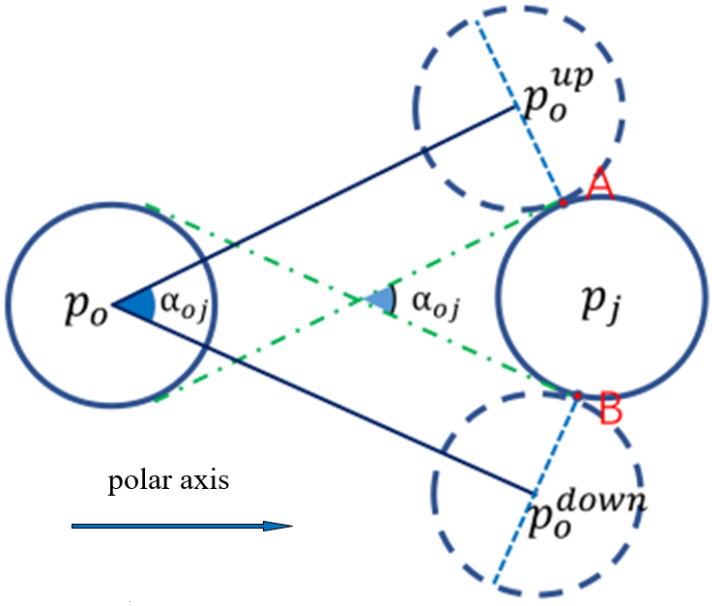

Figure 4. Schematic diagram of direction of lossless fruit separation in secondary adjacent regions.

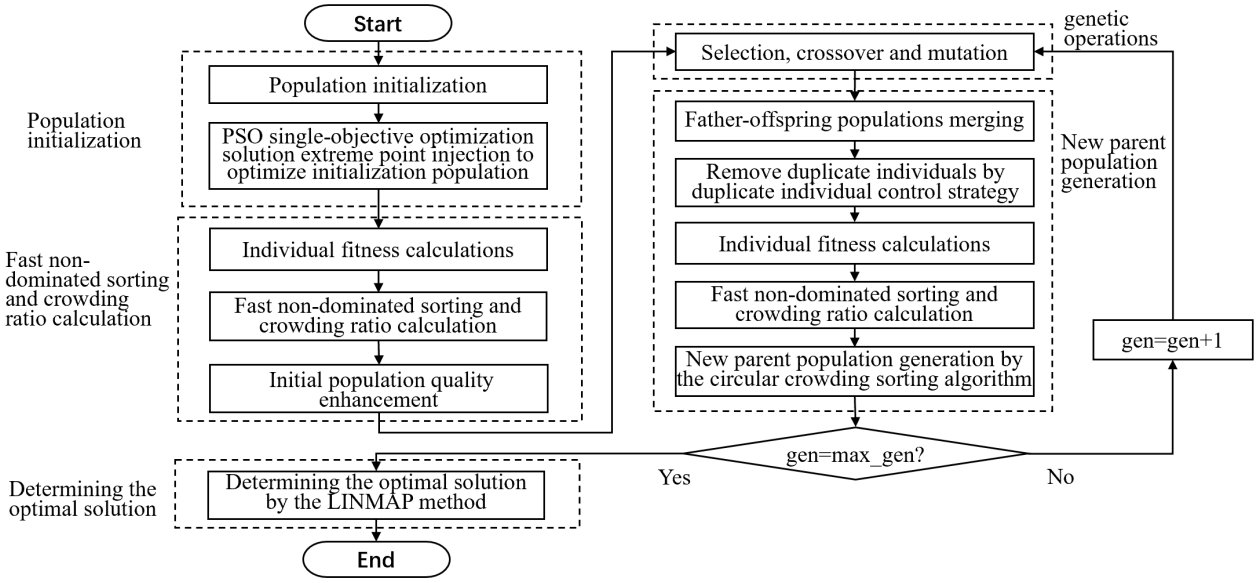

Figure 5. The algorithm flow of I-NSGA-II.

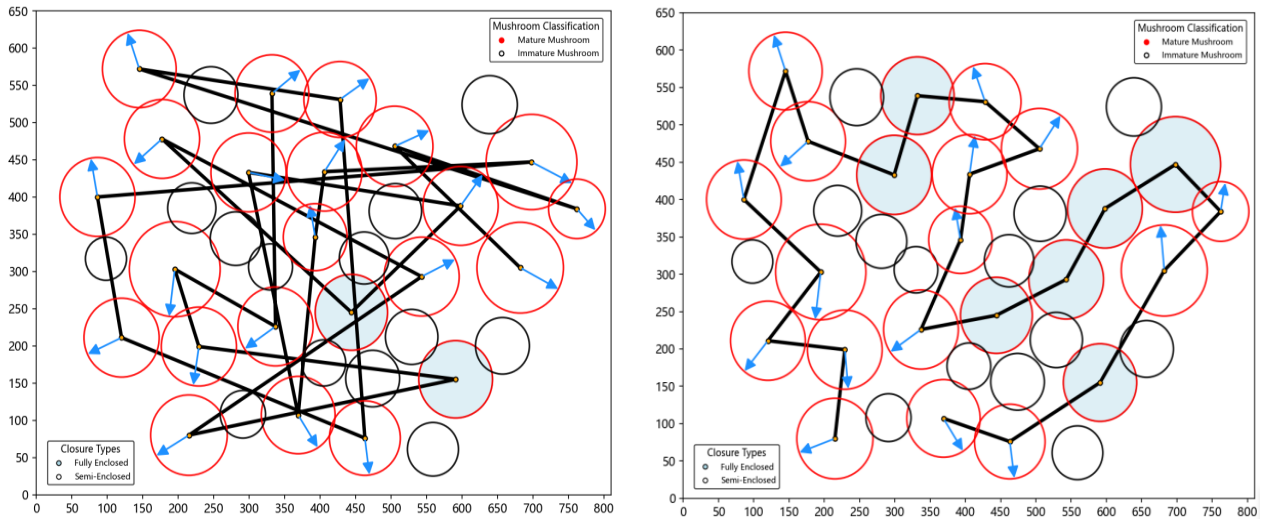

(a)Single goal optimization of picking path

(b)Single goal optimization of picking failure

Figure 6. Two effects of single-object optimization of picking sequence.

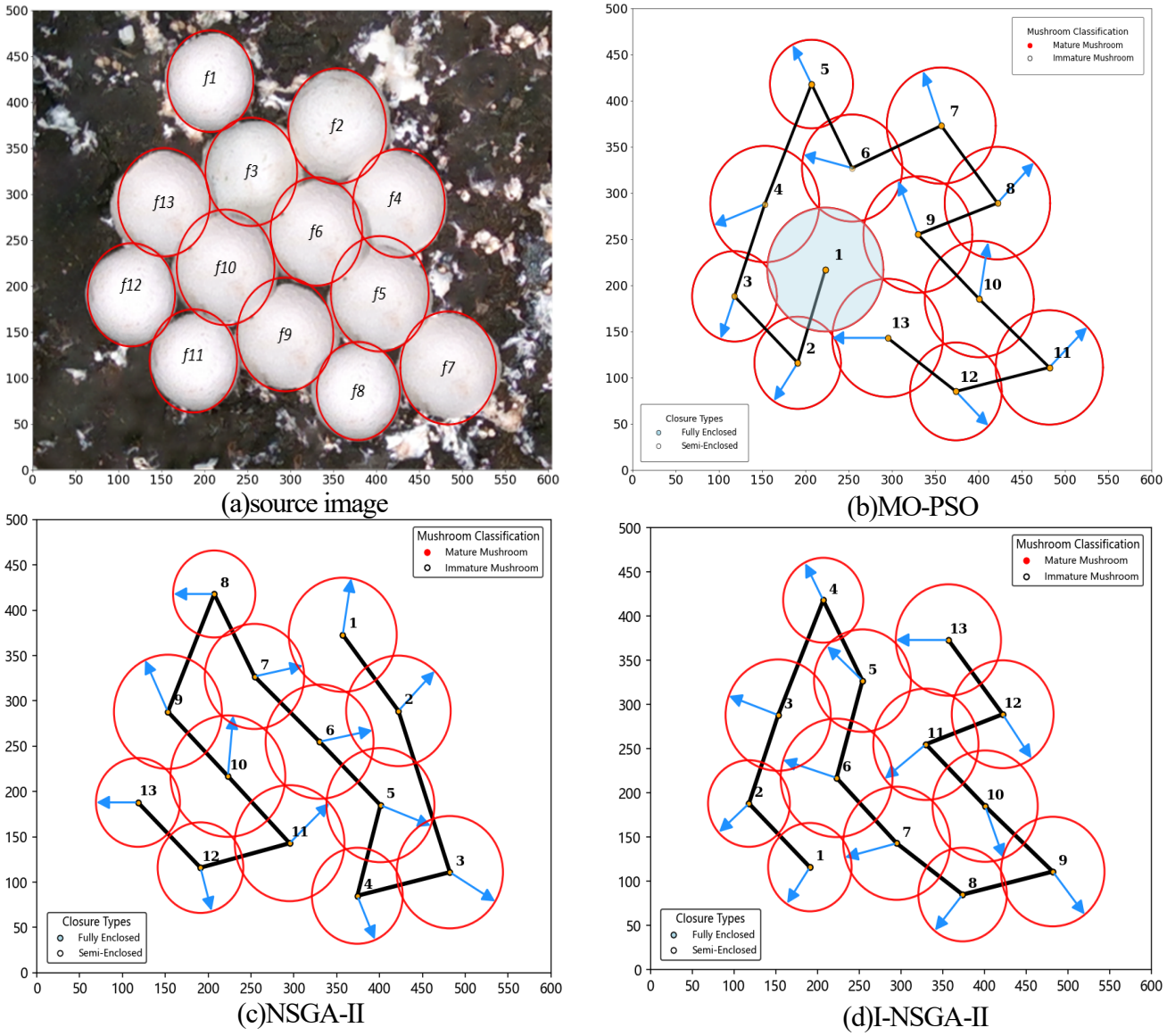

Figure 7. Schematic diagram of intensive cluster picking strategy containing only mature fruiting bodies after multi-objective optimization.

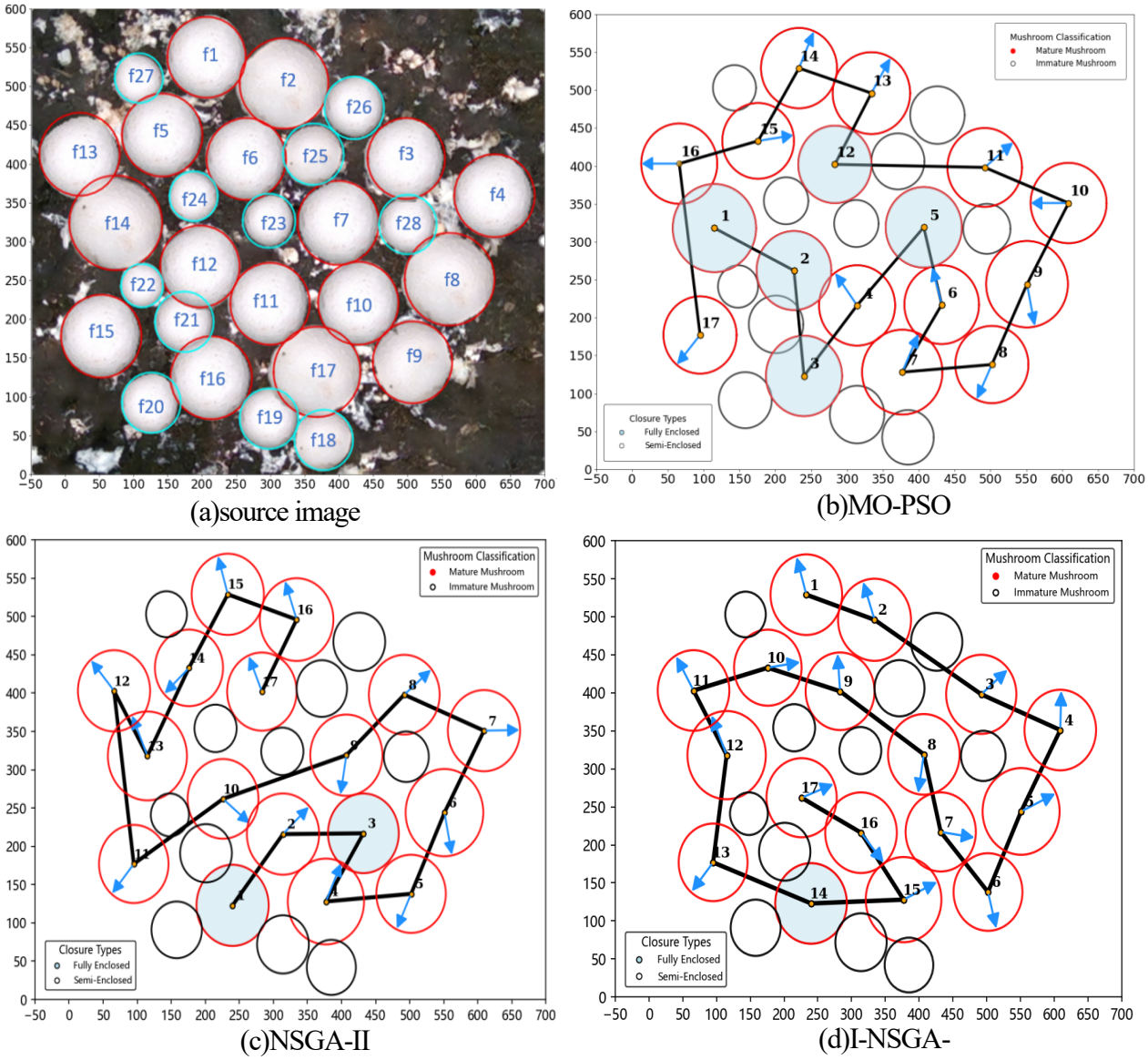

Figure 8. Schematic diagram of intensive sonic cluster picking strategy containing mature and immature sonic bodies after multi-objective optimization.

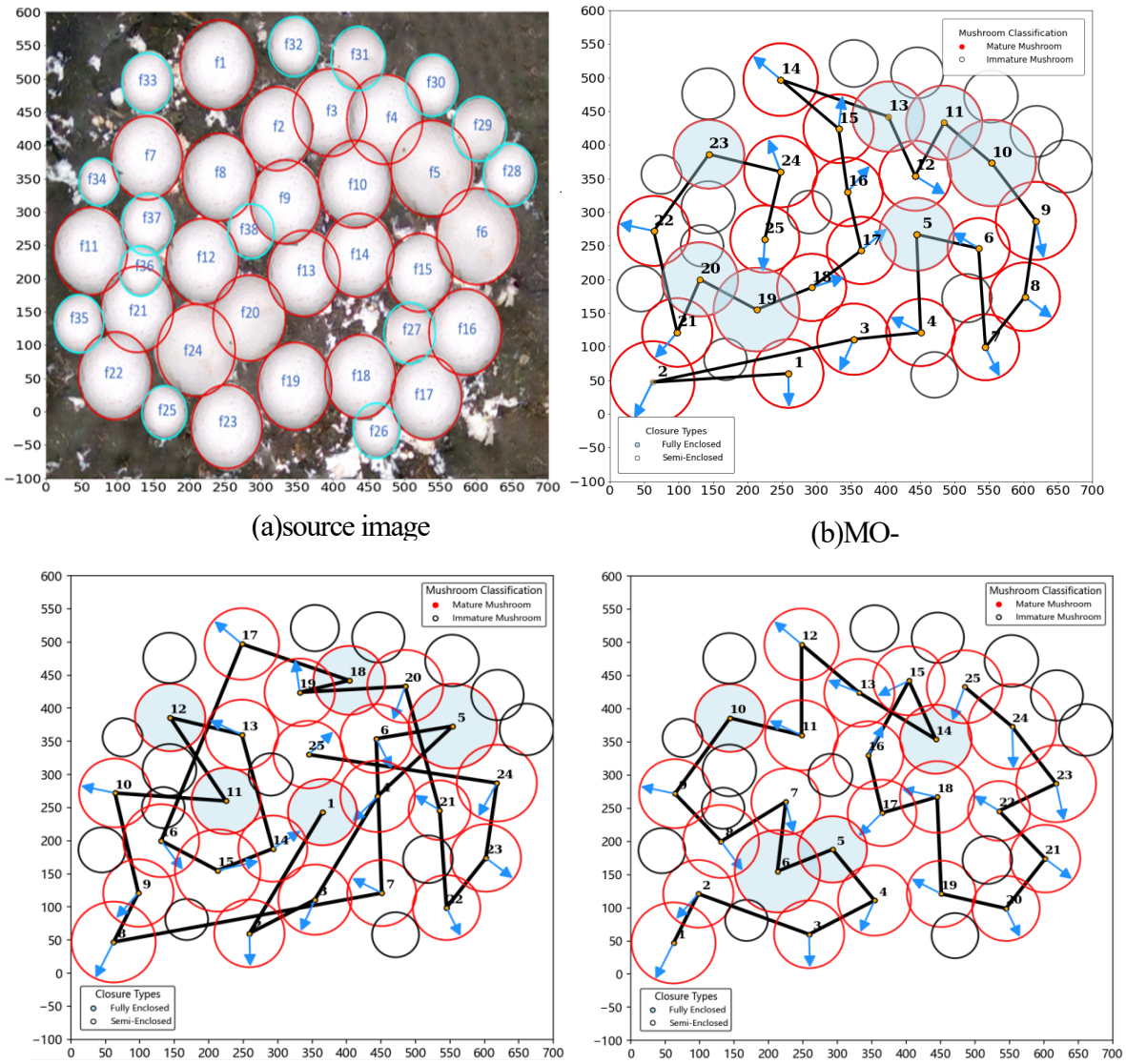

Figure 9. Schematic diagram of picking strategy for higher aggregation degree sub-entity cluster after multi-objective optimization

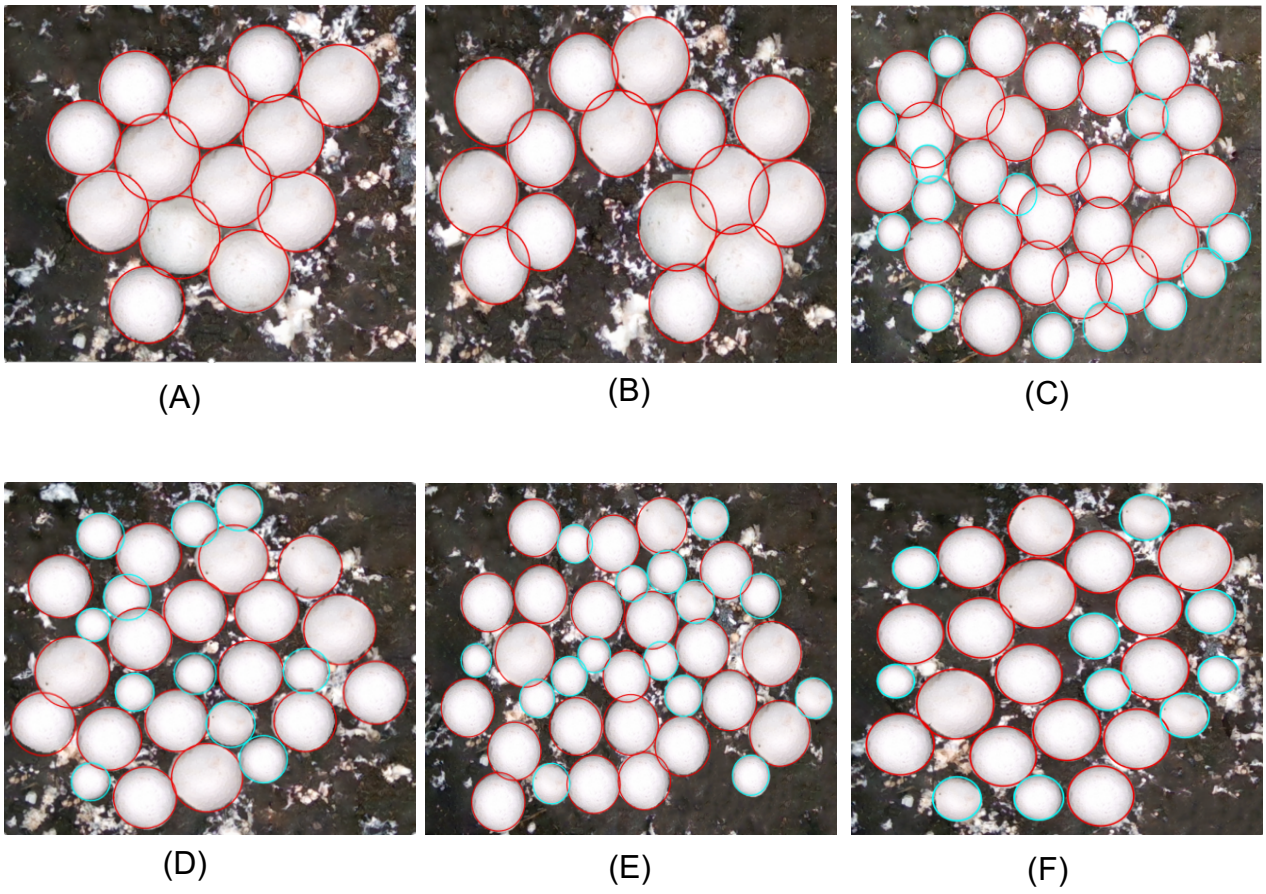

Figure 10. Original image of six group comparison experimental data set.

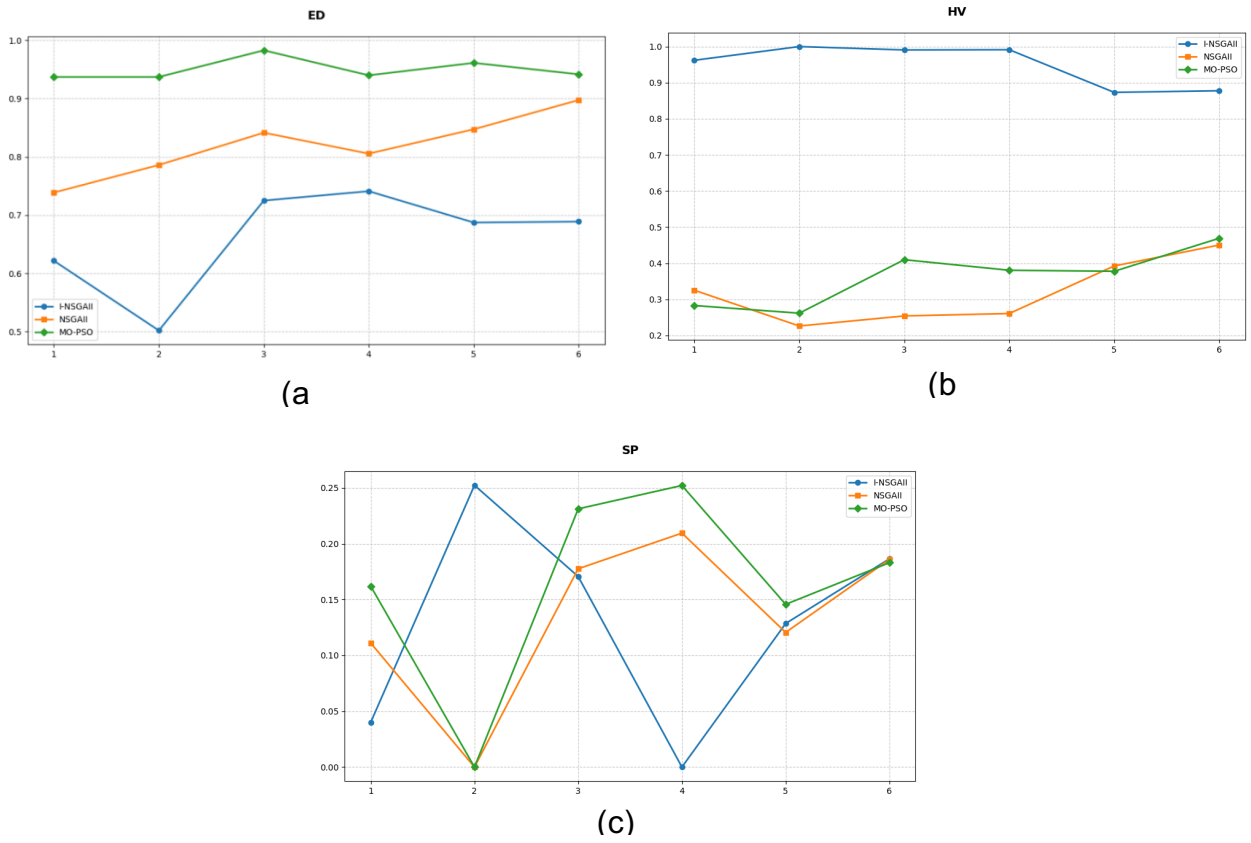

Figure 11. Comparison of indicators of each algorithm under each distribution.

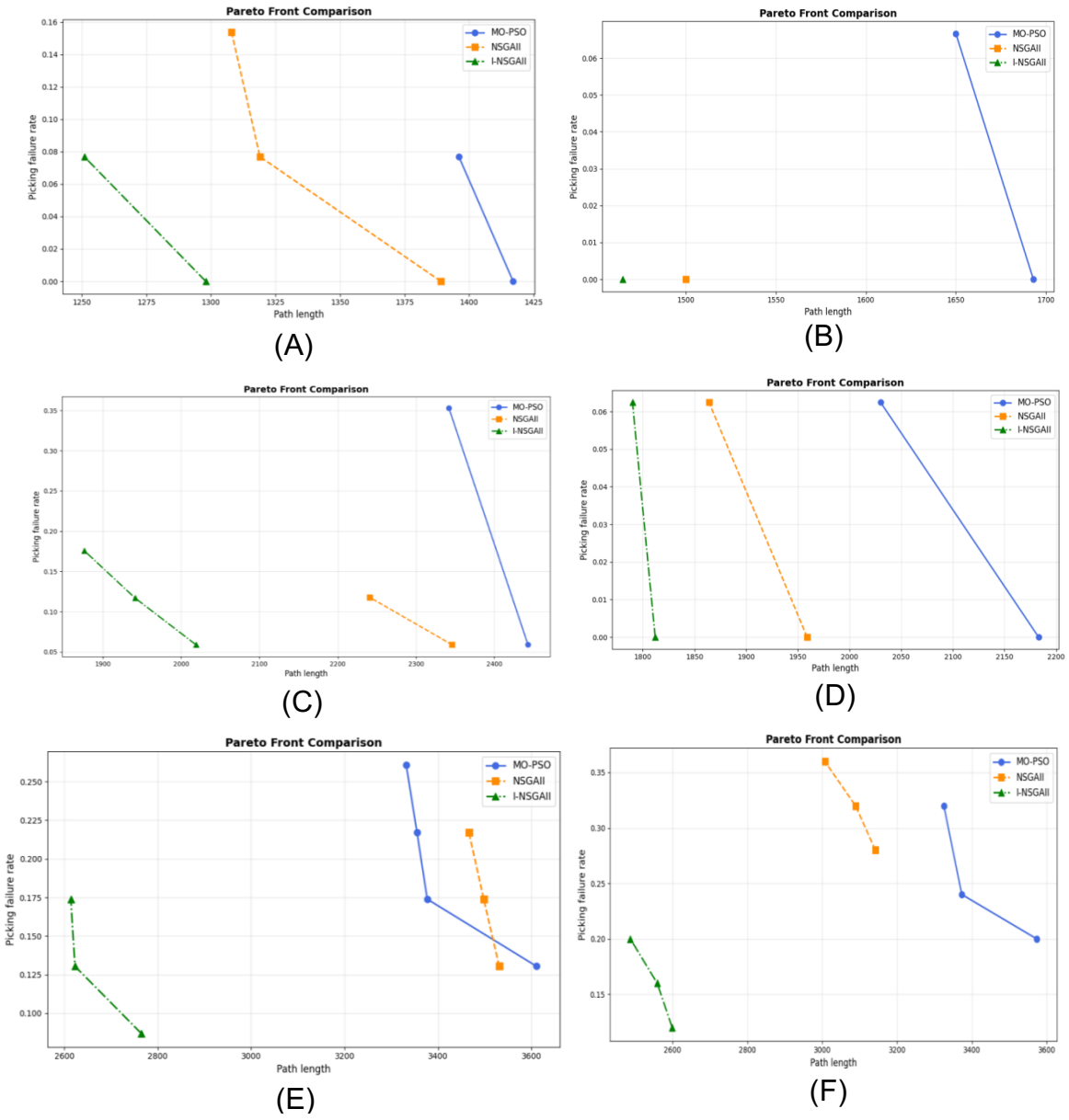

Figure 12. The Pareto frontier solution set distribution of each algorithm under different fruit density distribution.

Table 1. Results of experiment 1.

	Number of fruits without separable direction (pcs)	Non-destructive separation failure rate (%)	Length of picking path (mm)
Initial state	5	-	-
Optimizing non-destructive separation failure rate only (GA)	0	0	2300
MO-PSO	1	7.6	1396
NSGA-II	0	0	1504
I-NSGA-II	0	0	1390

Table 2. Results of experiment 2.

	Number of fruits without separable direction (pcs)	Non-destructive separation failure rate (%)	Length of picking path (mm)
Initial state	9	-	-
Optimizing non-destructive separation failure rate only (GA)	1	5.8	4236
MO-PSO	4	23.5	2113
NSGA-II	2	11.7	2211
I-NSGA-II	1	5.8	1998

Table 3. Results of experiment 3.

	Number of fruits without separable direction (pcs)	Non-destructive separation failure rate (%)	Length of picking path (mm)
Initial state	15	-	-
Optimizing non-destructive separation failure rate only (GA)	5	20	6142
MO-PSO	7	29.1	3312
NSGA-II	5	20.8	3414
I-NSGA-II	4	16.6	2722